JOURNAL OF MATERIALS SCIENCE 17 (1982) 3541–3548

Size of plastic region owing to blunting of the precrack tip and J_{Ic} value in several types of structural steels

HARUHIKO FUJITA, OSAMU KAMIYA, MANABU TANAKA
The Mining College, Akita University, Tegata-Gakuen-cho, Akita 010, Japan

In this study, a three-point bend J_{Ic} fracture-toughness test was carried out using four types of structural steels at room temperature. The values of $(\gamma_p)V$, which represent the width of the region where the voids are located just ahead of the crack tip, were measured by Beacham's method [9] with the help of a scanning electron microscope (SEM). The experimental (γ_p) values and the theoretical values obtained using the finite element method (FEM) or calculated from K at initiation are in good agreement. It was found that there is a certain linear relationship between $(\gamma_p)V$ and the stretched zone width (SZW), and an experimental relationship between J_{Ic} and $\sigma_{flow} \cdot (\gamma_p)V$ which may be expressed by the following equation:

$$J_{Ic} = 44.1 + 0.35\sigma_{flow} \cdot (\gamma_p)V_c \qquad \text{kJ m}^{-2},$$

where σ_{flow} is the average value of the yield stress and the ultimate tensile strength. $(\gamma_p)V_c$ represents the critical value of $(\gamma_p)V$. The numerical constant 44.1 kJ m^{-2} is considered to be a J_{Ic} value for brittle fracture of the material tested, according to the authors' previous results. It is possible to calculate J_{Ic} if $(\gamma_p)V_c$ can be measured.

1. Introduction

Recently, parameters based on the fracture mechanics have been used as a safety-criterion in the design of structures [2]. Fracture-toughness testing of J_{Ic} is frequently used because it is possible to apply it not only to brittle fracture but also to ductile fracture [6] while K_{Ic} testing is applied only to the brittle fracture. Another advantage of J_{Ic} over K_{Ic} is size economy [5]: the specimen size required in order to obtain a valid J_{Ic} is smaller than that for a valid K_{Ic}. It is possible to convert the valid J_{Ic} into K_{Ic} and to use it as a safety criterion. Meanwhile several investigators have used relationships J_{Ic} and CTOD [3] or J_{Ic} and SZW, where CTOD is crack tip opening displacement and SZW is the stretched zone width. CTOD and SZW are directly related to the blunting of the crack tip and therefore to J_{Ic} [4, 7, 8]. It has been found that there is a lack of experimental discussion about the relationship between the size of the plastic region just ahead of the precrack tip and the J_{Ic} fracture-toughness parameter. It is difficult to measure the size of the plastic region at the central part of the specimen thickness where the ductile fracture initiates, but it may be possible to measure the size of the plastic region using the following techniques: etching, recrystallization, and measurement of the void regions; all of which need thorough study. In this study, a three-point bend J_{Ic} fracture-toughness test was carried out using four types of structural steels at room temperature and the values of $(\gamma_p)V$, which represent the width of the region where the voids are located just ahead of the crack tip were measured according to Beachem's method. The values of $(\gamma_p)V$ were compared with values from the plastic region calculated by the finite element method (FEM) and that calculated from K_{in}

0022–2461/82/123541–08$03.46/0

TABLE IA Chemical composition of the steels used

Steels	C	Si	Mn	P	S	Ni	Cr	V	Mn	Cu
HT80	0.13	0.25	0.82	0.009	0.005	0.85	0.48	0.04	0.48	0.22
HT60	0.15	0.25	1.28	0.017	0.005	0.01	0.02	0.05	–	–
SM50	0.15	0.34	1.40	–	–	–	–	–	–	–
SS41	0.18	0.21	0.88	0.05	0.05	–	–	–	–	–

TABLE IB Mechanical properties of the steels used

Steels	Yield stress (MPa)	Tensile strength (MPa)	Elongation (%)
HT80	824	883	32
HT60	500	628	30
SM50	363	520	34
SS41	265	431	36

(which is the value of K at which the ductile crack initiates). Finally, the quantitative relationship between $(\gamma_p)V$ and J_{Ic} is discussed.

2. Experimental method

Chemical composition and the mechanical properties of the four types of structural steels used are listed in Tables IA and IB. Three-point bend specimens, whose geometry is shown in Fig. 1, were fabricated out of these steels according to an ASTM tentative method [1]. The longitudinal direction of specimens was parallel to the rolling direction and precracks were normal and lateral to the direction of the plate. Fatigue precracks were machined by an electro-hydraulic fatigue testing machine in the frequency range 50 to 100 Hz. The fatigue load was within the maximum load calculated by the ASTM tentative standard. It required from 100 to 300×10^3 cycles to propagate 1 mm of the fatigue precrack.

The experimental block diagram is shown in Fig. 2. The fracture toughness test of the three-point bend was carried out by an electro-hydraulic-type testing machine (maximum load 10 t) with a constant cross-head speed of 1 mm min^{-1} at room temperature. The ductile crack initiation was detected by an electrical potential method, which has already been investigated by the authors in a previous report [12]. It is ascertained that the value of J_{Ic} obtained by this method agrees with the value from the R-curve method. The J_{Ic} values are calculated from [1];

$$J_{Ic} = 2A/B \cdot b \quad (1)$$

where A is the area under load, load–point displacement record up to the crack intiation point in energy units, B is the specimen thickness and b is the initial uncracked ligament. Four or five specimens of each type of steel were loaded up to different stages of blunting and then unloaded. Some of these specimens were broken in a brittle manner at the liquid nitrogen temperature and the rest were fractured by fatigue loading.

Fig. 3a shows a sketch of the voids remaining on the fatigue or brittle fracture surface, and the width of the region $(\gamma_p)V$ (where voids are located in front on the blunting crack) was measured at the central part of the specimen thickness. This observation technique for voids has already been used by Beachem [9]. Further details have been added by the present authors: angular holes as illustrated in Fig. 3b are not voids but small cracks or inclusion marks coming out; spherical holes shown in Fig. 3c are considered to be voids, which are blunted by plastic deformation. The values of SZW were also measured using SEM. The shape of the

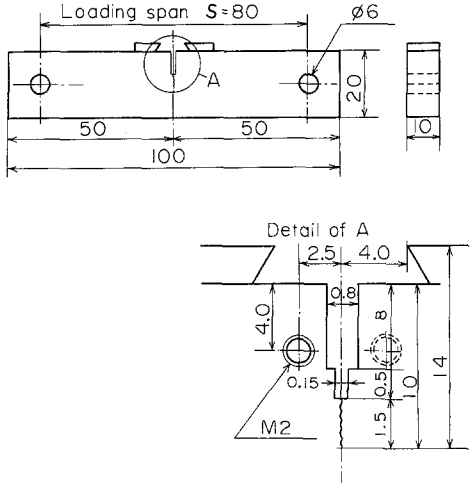

Figure 1 Geometry of a three-point bend specimen.

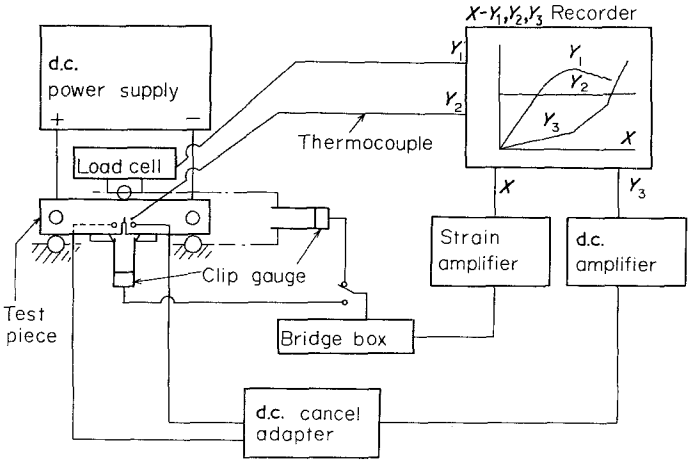

Figure 2 Block diagram for the electrical potential method.

plastic region was investigated by the recrystallizing heat-treatment, HT80, SM50, and SS41 steels were heated for 4 h at 963 K, HT60 steel was heated for 3 h at 1003 K and cooled in air.

3. Approach by the finite element method

The elastic–plastic analysis was carried out by the finite element method (FEM) [10] in order to discuss the extension of the plastic region with blunting of the precrack tip. Fig. 4 shows a finite element model of half the specimen, and Fig. 5 shows that of the cracked region using finer elements. The total number of elements and nodes is 462 and 267, respectively. The minimum side length of triangular elements around the crack tip is 0.1 mm. The stress condition is assumed to be plane strain in the calculation, and the strain-hardening characteristic of steel is represented by the following equation:

$$\bar{\sigma} = C(\alpha + \bar{\epsilon}_p)^n \qquad (2)$$

where $\bar{\sigma}$ and $\bar{\epsilon}_p$ are the von Mises' equivalent stress and strain, respectively. C, α, and n are materials constants and are listed in Table II. The materials used were assumed to be isotropic and to yield when the von Mises' equivalent stress $\bar{\sigma}$ reached 99% of the yield stress for each steel listed in Table II. The finite elements used incorporated a change in geometry with deformation by making a new stiffness matrix each time one element yielded.

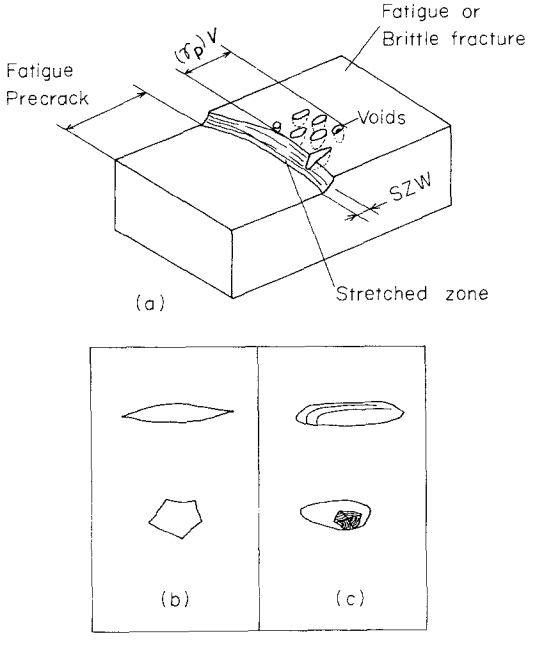

Figure 3 Sketches illustrating the void region $(\gamma_p)V$ and the distinction of voids.

4. Experimental results and discussion

4.1. Observation of voids in front of the precrack

The separation of inclusions from the matrix and the crack extension along the pearlite layer causes the formation of voids in a region where the yield

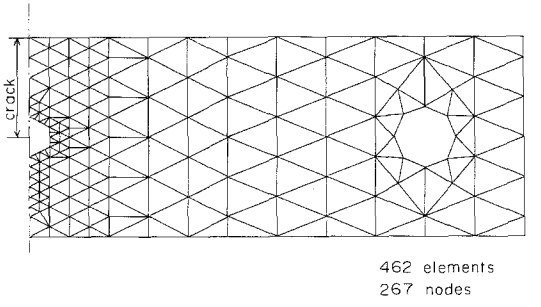

Figure 4 Finite element modelling of a three-point bend specimen using triangular membrane elements.

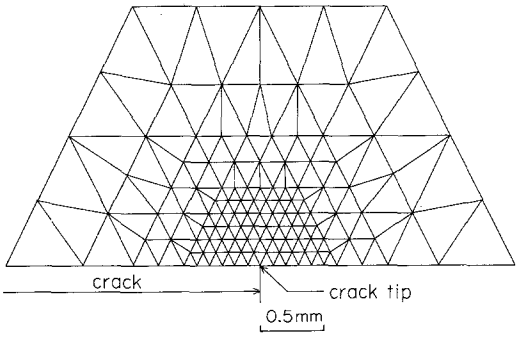

Figure 5 Finite element modelling of the crack region using triangular membrane elements.

TABLE II Material constants of steels

Steels	$\bar{\sigma} = C(\alpha + \bar{\epsilon}_p)^n$			Young's modulus, E (GPa)
	C	α	n	
HT80	109.2	0.005	0.046	205
HT60	84.0	0.010	0.094	206
SM50	92.0	0.006	0.184	206
SS41	71.8	0.005	0.208	206

stress is reached. The causes for the initiation of voids varied amongst the four types of steels used. Fig. 6a shows the HT80 steels surface fractured by fatigue loading after unloading from the crack initiation load. Fig. 6b shows the embryonic voids ahead of the crack tip in HT80 sectioned by cleavage fracture at low temperature after the three-point bend test at room temperature. The maximum size of these voids was 100 μm which was smaller than for the other steels. The inclusions, which are not very elongated and considered to be MnS, are nuclei of voids. Fig. 6c shows the voids of HT60, remaining on the surface fractured by fatigue; the maximum size of the voids was 200 μm which is bigger than that of HT80 because the voids were formed from MnS inclusions which had been sufficiently elongated. In SM50 steel, most of the voids were formed from the cracks along the pearlite layer, and some of them are greater than 300 μm in size, as shown in Fig. 6d. In SS41 steel, the ductile crack tips initiated from fatigue precracks are indistinctive because of the presence of voids caused by the pearlite layer and the inclusions. The growing process and size of the voids vary with the type of steel; however, it is considered that the stress should reach to the yield value at the region where these voids develop type I dimples. Therefore, there is a possibility that the size of the void region is equal to the yield region, in spite of the difference in growth process of voids in the steels used. The critical values of

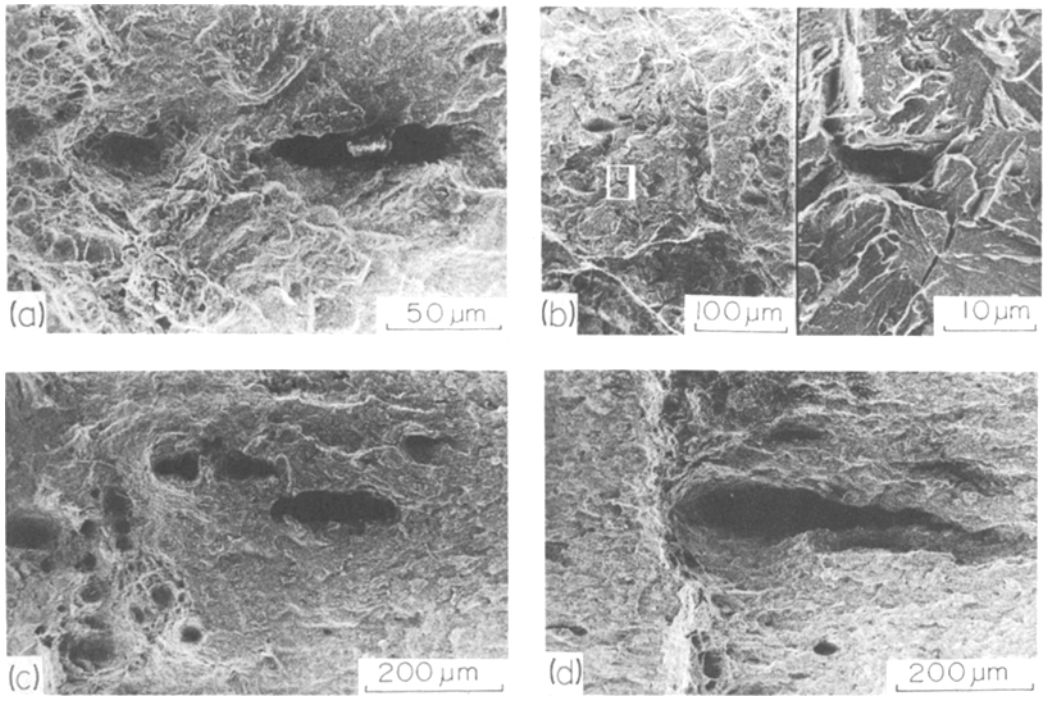

Figure 6 Scanning electron fractographs of voids ahead of crack tips in the steels tested. (a) HT80, (b) micro-void in HT80, (c) HT60, (d) SM50.

TABLE III Comparison between width of the region with voids and the yield region width calculated using FEM and K_{in}

Steels	Region with voids, $(\gamma_p)V_c$ (mm)	Yield region using FEM, $(\gamma_p)F_c$ (mm)	Yield region calculated from K_{in} $(\gamma_p)K_c$ (mm)
HT80	0.229	0.350	0.256
HT60	0.488	0.450	0.447
SM50	0.476	0.450	0.517
SS41	0.521	0.700	0.442

$(\gamma_p)V$ in the four types of steels, denoted by $(\gamma_p)V_c$ (the values at the time when the ductile crack initiation occurs at the central part of specimen) are listed in Table III.

4.2. The relationship between $(\gamma_p)V_c$ and the plastic region calculated using FEM and K_{in}

The load against load–point displacement curves and the plastic regions are shown in Figs. 7 to 10 for the steels used at room temperature. The calculated curves of load against load–point displacement are very close to the experimental ones in the elastic deformation. Advancing the plastic deformation at the precrack tip, in the real specimen, many voids and/or subcracks develop before the main crack initiates as shown in Fig. 6, so the crack opening and the load–point displacements are larger than the computed results. Double circles (◎) in these figures represent the initiation of ductile cracks detected by the electrical potential method. The curves of boundaries between elastic and plastic regions with parameter p (load) were found using FEM. The outermost curves, representing the plastic reions, correspond to the crack initiation load of each steel. These cuves are assumed to be the critical value of the plastic region, which increases with decreasing yield strength of the steels. The intersection of the curves and the X-axis of these co-ordinates is denoted by $(\gamma_p)F_c$. The values of $(\gamma_p)F_c$ are considered to be equal to the size of the plastic region in front of the precrack tip when the ductile crack initiates. When compared with the values of $(\gamma_p)V_c$ in Table III, $(\gamma_p)F_c$ values are nearly equal to $(\gamma_p)V_c$. Therefore, the value of the void region $(\gamma_p)V_c$ is considered to be the size of the plastic region.

The shape of the experimental plastic regions in SM50 and SS41 steels are shown by the recrystallization heat-treatment in Fig. 11. The shapes resemble to those of the plastic regions calculated using FEM but the size is smaller because the recrystallizing region represents 2% to 3% of the plastic strain according to our previous bending tests. It is found that the plane strain state assump-

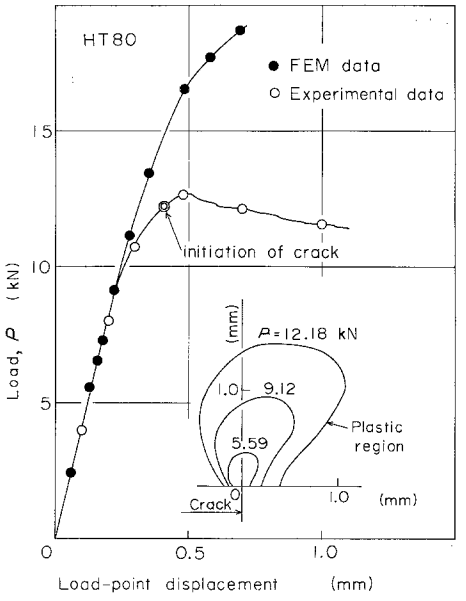

Figure 7 Plot of load against load–point displacement and plastic regions of HT80 steel at room temperature.

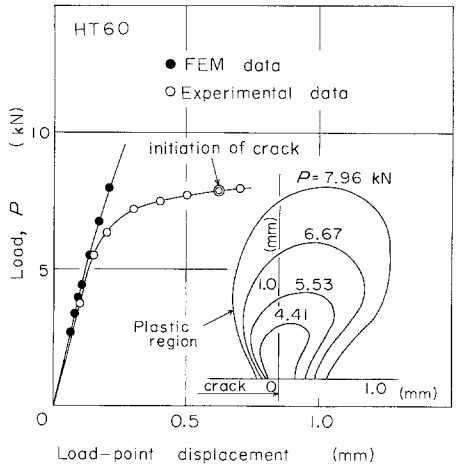

Figure 8 Plot of load against load–point displacement and plastic region of HT60 steel at room temperature.

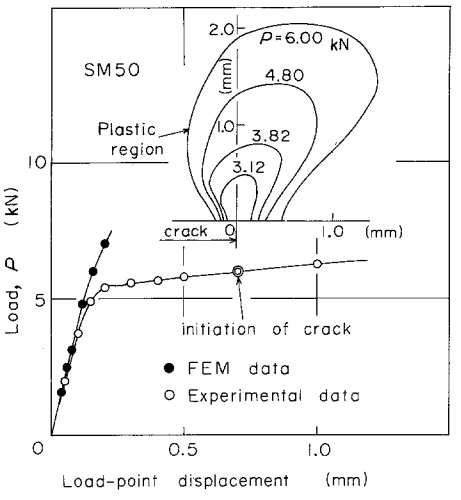

Figure 9 Plot of load against load–point displacement and plastic regions of SM50 steel at room temperature.

tion in the case of the calculation using FEM is valid because the shape of the plastic region resembles a butterfly wing which is a characteristic of the plane strain state.

The size of the plastic region, γ_p, can be calculated using the following equation, assuming that the plane strain state and Mode I conditions are maintained until the initiation of a ductile crack [11];

$$\gamma_p = \frac{1}{2\pi}\left(\frac{K_I}{\sigma_{ys}}\right)^2 \cos^2\left(\frac{\theta}{2}\right)\cdot\left[(1-2\nu)^2 + 3\sin^2\left(\frac{\theta}{2}\right)\right], \quad (3)$$

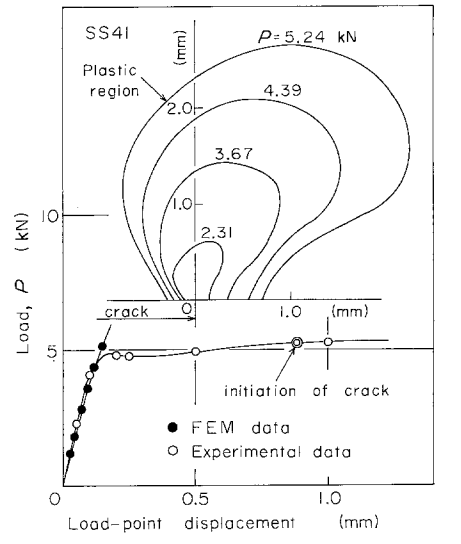

Figure 10 Plot of load against load–point displacement and plastic regions of SS41 steel at room temperature.

where $\gamma_p \ll C$, K_I is the stress intensity factor, σ_{ys} is the yield strength, θ is the angle between the directions of γ_p and the crack propagation, ν is the Poisson's ratio, and C is the crack length. The shape of the plastic region represented by this equation is also butterfly-wing shaped. Substitute K_{Ic} for K_I in Equation 3 and consider a direction ahead of the crack ($\theta = 0$).

$$(\gamma_p)K_c = \frac{(1-2\nu)^2}{2\pi}\left(\frac{K_{Ic}}{\sigma_{ys}}\right)^2. \quad (4)$$

The value of $(\gamma_p)K_c$ gives the critical size of the plastic region calculated using K_{Ic}. The $(\gamma_p)K_c$ results calculated for the four types of structural steels tested at room temperature are listed in Table III. It is found that the order of these values is equal to the experimental values of $(\gamma_p)V_c$.

4.3. Relationship between $(\gamma_p)V_c$, SZW, and J_{Ic}

Fig. 12 shows the relationship between the void region $(\gamma_p)V$ and SZW in the four types of steels. The values of SZW are the average ones in the central 4 mm portion of the specimen. A linear relation between $(\gamma_p)V$ and SZW is found in this figure. On the other hand, the relationship between SZW and J_{Ic} has been investigated by Kobayashi and co-workers [7]. In this study, the relationship between $(\gamma_p)V_c$ and J_{Ic} was investigated experimentally. Values of $(\gamma_p)V_c \cdot \sigma_{flow}$ were used as a parameter, where σ_{flow} is the average of the yield stress and the ultimate tensile strength.

Fig. 13 shows the relationship between $\sigma_{flow} \cdot (\gamma_p)V_c$ and J_{Ic}. It is found that there is a linear relationship between them given by:

$$J_{Ic} = 44.1 + 0.34\sigma_{flow} \cdot (\gamma_p)V_c. \quad (6)$$

The numerical constant 44.1 kJ m^{-2} in this equation is of the same order as the J_{Ic} value for brittle fracture in the authors' previous paper [12].

From these discussions, it is evident that the void region $(\gamma_p)V$ is nearly equal to the size of the plastic region and it is possible to calculate J_{Ic} by an experimental equation such as Equation 2, if $(\gamma_p)V_c$ can be measured.

5. Conclusions

Fracture-toughness testing of three-point bend pieces was carried out on four types of structural steels at room temperature and then the width of the void region $(\gamma_p)V$ was measured by the fracto-

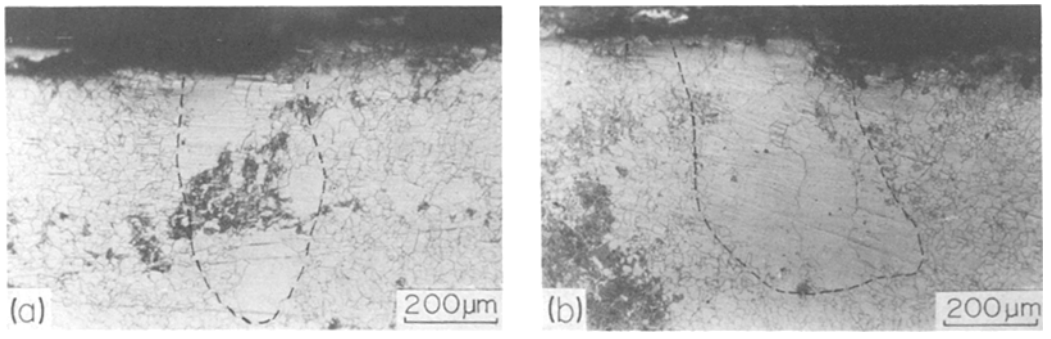

Figure 11 The plastic region found using the recrystallizing method. (a) SS41, (b) SM50.

graphic method. The values were compared with the results calculated from FEM and K_{in} values. The relationships between $(\gamma_p)V$, SZW, and J_{Ic} were investigated. The results obtained are summarized as follows.

(1) The critical size of the void region $(\gamma_p)V_c$ which is measured by Beachem's method, is nearly equal to the size of the plastic region calculated using FEM and K_{in} values.

(2) The values of $(\gamma_p)V_c$ increases with decreasing strength of the steels at room temperature.

(3) It was found that $(\gamma_p)V$ is proportional to the SZW. It is considered that the value of $(\gamma_p)V$ is one of the new parameters corresponding to the blunting at the precrack tip.

(4) The value of $(\gamma_p)V_c$ and the fracture toughness value of J_{Ic} measured by the electrical potential method are related by the following equation:

$$J_{Ic} = 44.1 + 0.34\sigma_{flow} \cdot (\gamma_p)V_c \quad \text{kJ m}^{-2}.$$

The numerical constant 44.1 kJ m^{-2} corresponds to the values of J_{Ic} when brittle fracture occurs. It is found that it is possible to calculate J_{Ic} by an experimental equation, as mentioned previously, if $(\gamma_p)V_c$ can be measured.

Acknowledgements

The authors acknowledge the experimental assistance given by Mr A. Takahashi and Mr Anda Augusto and the technical assistance given by Mr F. Ashihara. The authors would like to thank Nippon Steel Corporation for supplying the material used in this study.

References

1. ASTM Standard, "The Determination of J_{Ic}, a Measure of Fracture Toughness" (ASTM, Philadelphia, 1980).
2. J. D. HARRISON, *J. Japan Weld. Soc.* 49 (1980) 6 (in Japanese).
3. BS5762 (1979).
4. T. HOLLSTEIN and J. G. BLAUEL, *Int. J. Fract.* 13 (1977) 385.
5. W. L. SERVER, R. A. WULLAERT and R. O. RITCHIE, *Trans. ASME. J. Eng. Mater. Tech.* 102 (1980) 192.

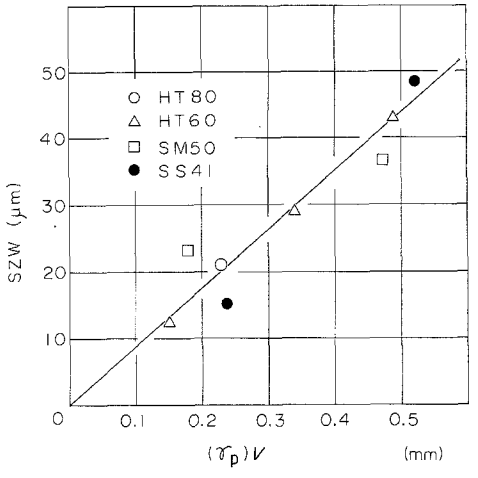

Figure 12 Relationship between SZW and the void region width $(\gamma_p)V$ of the steels at room temperature.

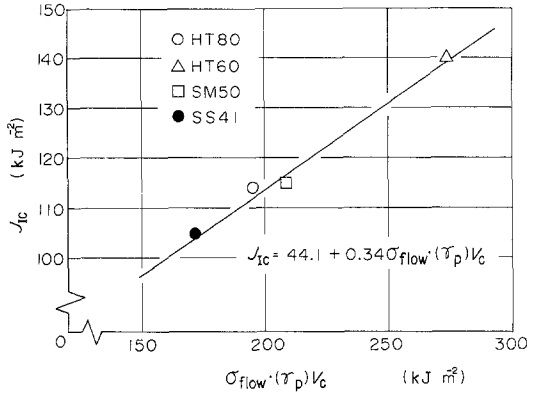

Figure 13 Relationship between J_{Ic} and $\sigma_{flow} \cdot (\gamma_p)V_c$ of steels at room temperature.

6. J. A. JOYCE and D. F. HASSON, *Eng. Fract. Mech.* **13** (1980) 417.
7. H. NAKAMURA, H. KOBAYASHI and N. NAKAZAWA, *Zairyo* **29** (1980) 533 (in Japanese).
8. K. OHJI, K. OGURA, H. UCHIDA and T. FUJIMOTO, Preprint, *Japan Soc. Mech. Eng.* No790-2 (1974) 168 (in Japanese).
9. C. D. BEACHEM, T. C. LUPTON and B. F. BROWN, *Met. Trans.* **2** (1971) 141.
10. Y. YAMADA, "Sosei-Nendansei (Plasticity-viscoelasticity)", (Baihukan, Tokyo, 1972) p. 173.
11. H. NAKAZAWA and H. KOBAYASHI, "Kotai-no-Kyodo (Strength of solids)" (Kyoritsu-press, Tokyo, 1976) p. 126.
12. H. FUJITA, M. TANAKA and O. KAMIYA, *Tesu to Hagane* **67** (1981) 382 (in Japanese).

Received 4 January
and accepted 17 May 1982